Available online at www.sciencedirect.com
SCIENCE DIRECT®
International Journal of Heat and Mass Transfer 49 (2006) 718–726
International Journal of HEAT and MASS TRANSFER
www.elsevier.com/locate/ijhmt

Numerical analysis of entropy generation and optimal Reynolds number for developing laminar forced convection in double-sine ducts with various aspect ratios

T.H. Ko *

Department of Mechanical Engineering, Lunghwa University of Science and Technology, 300, Wan-Shou Rd. Sec. 1, Kueishan, 33306 Taoyuan, Taiwan

Received 28 September 2004; received in revised form 17 August 2005
Available online 14 October 2005

Abstract

In the present paper, the entropy generation in a double-sine duct, which is frequently used in plate heat exchangers, is investigated by numerical methods. The Reynolds number (Re) at inlet covers ranges from 86 to 2000, and wall heat flux (q'') varies as 160, 320 and 640 W/m^2. Three aspect ratio (Λ/a) cases, including $\Lambda/a = 2$, 4 and 8, are investigated. The results indicate that the entropy generation, S^*_{gen}, in cases with larger Re and smaller q'' is dominated by the entropy generation due to frictional irreversibility (S^*_P); whereas the entropy generation is dominated by the entropy generation due to heat transfer irreversibility (S^*_T) in cases with smaller Re and larger q''. There is no monotonic relationship between Λ/a and S^*_P or S^*_T. For all cases with different Re and q'', S^*_P is found to be minimal in $\Lambda/a = 2$ case, whereas S^*_T is minimal in $\Lambda/a = 4$ case. The optimal aspect ratio, $(\Lambda/a)_{opt}$, with which the minimal S^*_{gen} can be obtained, is found to be dependent on Re and q''. In $q'' = 160$ W/m^2 case, $(\Lambda/a)_{opt} = 2$ when $Re > 540$; $(\Lambda/a)_{opt} = 4$ when $Re < 540$. In $q'' = 320$ W/m^2 case, $(\Lambda/a)_{opt} = 2$ when $Re > 662$; $(\Lambda/a)_{opt} = 4$ when $Re < 662$. In $q'' = 640$ W/m^2 case, $(\Lambda/a)_{opt} = 2$ when $Re > 1008$; $(\Lambda/a)_{opt} = 4$ when $Re < 1008$. An optimal Re, which is found to increase with q'', exists for every case with specific Λ/a and q'' to induce the minimal S^*_{gen}. These results provide important information for the heat exchanger design since the thermal system could have the least irreversibility and best exergy utilization if the optimal Re and optimal aspect ratio is used according to the practical design conditions.

Keywords: Entropy generation; Double-sine duct; Aspect ratio; Irreversibility; Exergy

1. Introduction

Plate heat exchangers are extensively employed in food, pharmaceutical, chemical processing and many other industrial applications. Among the great variety of possible corrugation patterns of the plate surface, the chevron wave types have been proved to be a successful design with good heat transfer performance, in which the corrugation with the sinusoidal profile, as shown in Fig. 1, is the most widely used pattern. Because of practical importance, abundant works have focused on the heat transfer and fluid dynamics in chevron-type plate heat exchangers in last several decades, and most of the previous studies were experimental in nature. The review works by Shah and Focke [1] provided a good survey of such studies. Focke et al. [2] and Heavner et al. [3] systematically analyzed the effect of the corrugation inclination angle on the thermal-hydraulic performance of the heat exchanger by investigating experimental data in previous literatures. Martin [4] recommended the correlations of friction factors and heat-transfer coefficient for plate heat exchangers as functions of the corrugation inclination angle and Reynolds number, which were very useful for the practical design work. The analytical or numerical studies on plate heat exchangers are relatively rare. Ding and Manglik [5] and Manglik and Ding [6] used the Galerkin

* Tel.: +886 2 82093211; fax: +886 2 82091475.
E-mail address: thko@mail.lhu.edu.tw

0017-9310/$ - see front matter © 2005 Elsevier Ltd. All rights reserved.
doi:10.1016/j.ijheatmasstransfer.2005.08.023

Nomenclature

a	half amplitude of the sinusoidal corrugation (mm)
C_P	specific heat capacity (kJ/kg K)
d_h	hydraulic diameter (m)
f	friction factor
$\bar{h}$	average heat transfer coefficient in the duct (W/m^2 K)
k	thermal conductivity (W/m K)
L	distance between the centers of the upper and lower port holes of the chevron plate (m)
Nu	average Nusselt number
P	pressure (kpa)
q''	wall heat flux (W/m^2)
$\dot{Q}$	heat transfer rate (W)
Re	Reynolds number
S'''_P	volumetric entropy generation rate due to friction (W/m^3 K)
S'''_T	volumetric entropy generation rate due to heat transfer (W/m^3 K)
S'''_{gen}	total volumetric entropy generation rate due to heat transfer (W/m^3 K)
S^*_P	non-dimensional entropy generation rate due to friction
S^*_T	non-dimensional entropy generation rate due to heat transfer
S^*_{gen}	non-dimensional entropy generation rate
T	temperature (K)
T_0	temperature at axial entrance (K)
T_b	bulk mean temperature on a $z =$ constant cross-sectional plane (K)
T_W	wall temperature (K)
u	velocity component in x-direction (m/s)
V	average velocity in duct (m/s)
v	velocity component in y-direction (m/s)
w	velocity component in z-direction (m/s)
x	coordinate (m)
y	coordinate (m)
z	coordinate (m)
Φ	the area enlargement factor
Λ	wavelength of the sinusoidal corrugation (mm)
μ	molecular viscosity (kg/m s)
β	chevron inclination angle
ρ	density (kg/m^3)

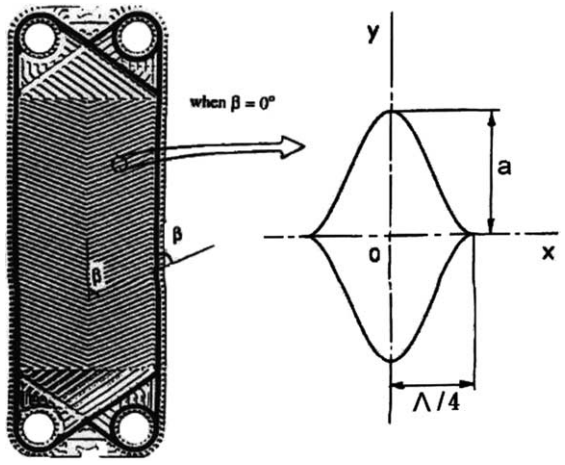

Fig. 1. The configuration and coordinate system of a chevron heat exchanger and double-sine duct.

function-based integral method to get the analytical solutions of two-dimensional laminar, fully developed flows in double-sine ducts. Fisher and Martin [7] numerically analyzed the friction factors for fully developed laminar flow in ducts confined by corrugated parallel walls by using the finite element method. Jang and Lin [8] carried out a numerical analysis of the three-dimensional heat transfer and fluid flow in chevron plate channels, in which the effect of corrugation inclination angle was emphasized.

For heat exchanger designs, the improvement of heat transfer performance is the most important work. However, the designers and engineers face a conflict problem that the heat transfer enhancement is always achieved at expense of the increase of friction loss; therefore, the optimal trade-off by selecting the most appropriate configuration and the best flow conditions has become one of the critical challenges for current design work. Recently, exergy has been used as a gauge to evaluate the performance of a thermal system. The analysis of the exergy utilization and the entropy generation has become one of the primary objectives in designing a thermal system. The contemporary trend in the field of heat transfer and thermal design must include the consideration of thermodynamic Second-law, the design-related concept of efficient use of exergy and the minimization of entropy generation [9]. Bejan [10] has described the systematic methodology of computing entropy generation through heat and fluid flow in heat exchangers. Based on the entropy generation minimization principle, considerable optimal designs of thermal systems have been proposed. For example, the optimization for convective heat transfer through a duct with constant heat flux by Nag and Naresh [11]; the irreversibility analysis in various duct geometries with constant wall heat flux and laminar flow by Sahin [12]; the investigation of entropy generation and pumping power in a turbulent fluid flow through a smooth pipe subjected to constant heat flux by Sahin [13]; the optimal design of the fin geometry in an

electronics cooling system based on the exergoeconomic analysis by Shuja [14], and the series optimal design of helical coils with laminar forced convection proposed by Ko and Ting [15,16] and Ko [17].

Similar with other thermal systems, there are several important parameters to have significant influences on heat and momentum transport phenomena in plate heat exchangers. These parameters contribute to irreversibility and entropy generations usually compete with one another inherently. Therefore, the optimal design of the plate heat exchangers with the best configuration and operating performance should exist and could be determined by choosing the optimal combination of these parameters through exergy analysis. However, from the view point of thermodynamics, all of the above-mentioned articles related to the plate heat exchangers are restricted to only thermodynamic First-law analysis, based on which the optimal design of the heat exchangers can not be achieved. To the best knowledge of us, the optimizing work of the plate heat exchangers by using the minimal entropy generation concept has never been explored in previous literatures; nonetheless, the investigation of the thermodynamic optimal design of the plate heat exchangers through the exergy analysis should be worthwhile for practical applications.

When the chevron inclination angle β equals to zero and the corrugations of the two plates are phase shifted by π (see Fig. 1), the straight longitudinal flow in a number of parallel channels with a double-sine cross section are obtained. Since the flow configuration represents a limiting case for the heat enhancement due to the chevron plates, the relevant studies on the case have been carried out by many researchers [4–6], but only limited to the thermodynamic first law. In view of the above arguments, the present paper is conducted to perform the optimizing work by analyzing the entropy generation in a double-sine duct with developing laminar convection and constant wall heat flux. An attempt has been made in the paper to find the optimum Reynolds number and aspect ratio based on the entropy generation minimization principle.

2. Configuration and parameters of a chevron plate heat exchanger

Fig. 1 shows the flow cross-sectional geometry and coordinate system for a double-sine shaped duct in a typical chevron plate passages ($\beta = 0°$). The principal geometric dimensions include the amplitude of the sinusoidal corrugation, $2a$, and the wavelength, Λ. The vertical length of a plate, L is measured between the centers of the upper and lower port holes. The characteristic length for the present problem is the hydraulic diameter, d_h, which is defined as

$$d_h = 2a/\Phi$$

where Φ is called the area enlargement factor and equals to the ratio of the developed surface area to the projected area. Reynolds number (Re) and Nusselt number (Nu), are defined as follows:

$$Re = \rho V d_h/\mu, \quad Nu = \bar{h} d_h/k$$

where V and $\bar{h}$ are the average velocity and average heat transfer coefficient in the chevron plate. Air has been selected as working fluid in current studies. The thermophysical properties of molecular viscosity (μ), thermal conductivity (k) and density (ρ) are 1.846×10^{-5} kg/m s, 0.0263 w/m K and 1.161 kg/m^3, respectively. For all the calculated cases, L is fixed as 100 mm, which is large enough for setting the outlet boundary condition. The Reynolds number at inlet covers ranges from 86 to 2000, and wall heat flux q'' varies as 160, 320 and 640 W/m^2. Three aspect ratio cases, including $\Lambda/a = 2$, 4 and 8, are investigated.

3. Mathematical model and numerical methods

3.1. Mathematical model

The present problem includes the developing region, and is assumed as three-dimensional, laminar, incompressible and steady. The continuity equation, Navier–Stokes equation and energy equation are solved simultaneously. These equations in tensor form are as follows:

$$\frac{\partial U_i}{\partial x_i} = 0 \tag{1}$$

$$\frac{\partial}{\partial x_j}(\rho U_i U_j) = -\frac{\partial P}{\partial x_j} + \frac{\partial}{\partial x_j}\left[\mu\left(\frac{\partial U_i}{\partial x_j} + \frac{\partial U_j}{\partial x_i}\right)\right] \tag{2}$$

$$\frac{\partial}{\partial x_j}\left(\rho U_j C_P T - k\frac{\partial T}{\partial x_j}\right) = U_j\frac{\partial P}{\partial x_j} + \mu\left(\frac{\partial U_i}{\partial x_j} + \frac{\partial U_j}{\partial x_i}\right)\frac{\partial U_i}{\partial x_j} \tag{3}$$

Because of the symmetric configuration, only 1/4 part of the duct is calculated. On the two symmetric planes ($x = 0$ and $y = 0$ planes), the boundary conditions are set as follows. On $x = 0$ plane: $u = 0$ and $\partial\phi/\partial x = 0$; ϕ represents v, w, P and T. On $y = 0$ plane: $v = 0$ and $\partial\phi/\partial y = 0$; ϕ represents u, w, P and T. At inlet, i.e. $z = 0$ plane, only the axial velocity component is non-zero, and the velocity distribution is assumed to be uniform for simplicity. At outlet, i.e. $z = L$ plane, the flow is assumed to be fully developed. The diffusion fluxes in the direction perpendicular to the outlet plane for three velocity components and T are set to zero. The suitability of the fully developed condition set at the duct outlet will be discussed later. On all walls, non-slip conditions and constant heat flux are specified. As the velocity and temperature distributions of the flow field are solved, the friction factor, f, and Nusselt number, Nu, can be calculated as follows:

$$f = \frac{1}{2}\frac{d_h}{\rho V^2}\left(-\frac{dP}{dz}\right) \tag{4}$$

Local Nusselt number at a $z =$ constant position

$$Nu = q'' d_h/k(T_W - T_b) \tag{5}$$

where T_W and T_b are the average wall temperature and bulk mean temperature on a cross-sectional plane at a specific z position

$$T_b = \frac{1}{VA}\int_0^A wT\,dA. \tag{6}$$

In addition, the volumetric entropy generation due to the heat transfer (S'''_T) and friction (S'''_P) can be calculated by the following equations [10]:

$$S'''_T = \frac{k}{T^2}(|\nabla T|)^2 \tag{7}$$

$$S'''_P = \frac{\mu}{T}\left(\frac{\partial U_i}{\partial x_j}+\frac{\partial U_j}{\partial x_i}\right)\frac{\partial U_i}{\partial x_j}. \tag{8}$$

The total volumetric entropy generation in the flow field can be obtained by

$$S'''_{gen} = S'''_T + S'''_P \tag{9}$$

3.2. Numerical method

The unstructured grid system is used for the present computations. All the above-mentioned equations accompanied with boundary conditions are discretized by a finite volume formulation. In the equations, the convective terms are modeled by the secondary-order upwind scheme; meanwhile the diffusive terms are modeled by the central difference scheme. The numerical solution procedure adopts the well-known semi-implicit SIMPLE algorithm, which was developed by Launder and Spalding [18]. All the detailed numerical procedure can be found in [19]. The convergent criteria is set as the relative residual of all variables, including mass, all velocity components and temperature less than 10^{-5}. A well-validated CFD software CFD RC (ESI US R&D, Inc.) is used for the numerical solutions.

4. Results and discussion

4.1. Grid independent test and code validation

For grid independent test, three grid systems, including 33,417, 59,697 and 119,997 grids, are adopted to calculate a baseline case with $\Lambda/a = 4$. Fig. 2 shows the Nusselt number at fully developed condition for the case calculated by the three grid systems, from which the difference between the results of 59,697 and 119,997 grids are found to be very limited. Therefore, 59,697 grids are concluded as dense enough to get the grid independent solutions. In the following cases, the grid system with 59,697 grids is used.

For validating the accuracy of numerical solutions, the friction factor and Nusselt number under fully developed condition from the present numerical solutions are compared with the Newtonian fluid cases of the analytical solutions presented by Manglik and Ding [6], which were obtained based on the Galerkin integral method. The comparisons cover three cases of $\Lambda/a = 2$, 4 and 8. Fig. 3 shows the axial distributions of Nu from numerical solutions for the three cases, which include the developing region as well as the fully developed region. For all the three cases, Nu is found to decrease with a sharp slope immediately as fluids enter the channel entrance, and reaches a constant magnitude very quickly. The results reveal the computational domain with axial length of 100 mm is long enough for setting the outlet condition as zero diffusive flux at duct exit. The comparisons of fully developed friction factor and Nu for the three cases are shown in Figs. 4 and 5, respectively, from which the numerical prediction of friction factor is nearly coincident with the analytical solution; however, there is some minor difference between the numerical and analytical solutions of Nu in $\Lambda/a = 2$ and 8 cases. The deviation may be resulted from numerical errors or the influences of axial conduction and viscous dissipation terms in energy equation, which are neglected in the analytical solution but are included in the present numerical solutions. Nonetheless, the difference is very limited, and the numerical solution is verified to have reasonable accuracy.

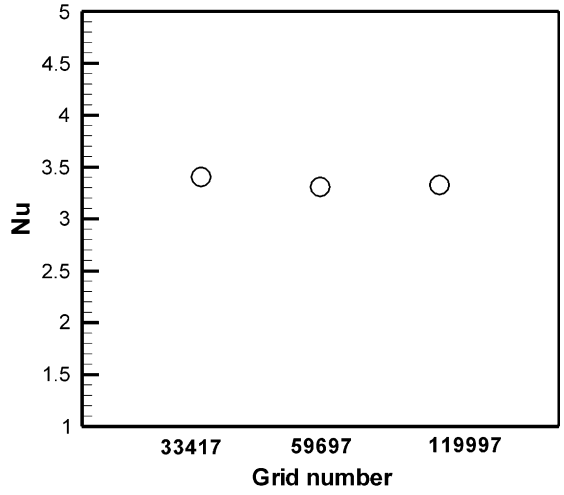

Fig. 2. Predicted Nusselt number at fully developed condition by different grid systems.

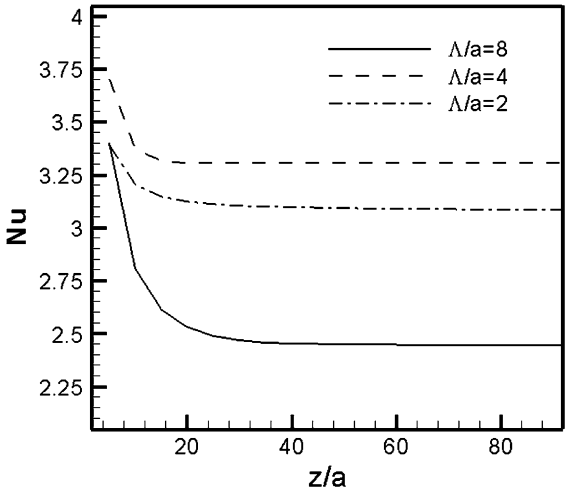

Fig. 3. The predicted axial distributions of Nu for $\Lambda/a = 2$, 4 and 8 cases.

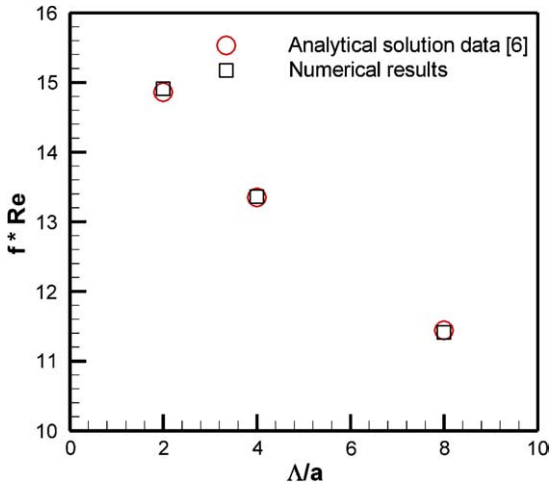

Fig. 4. The comparisons of friction factor at fully developed condition by numerical prediction and analytical solution for $\Lambda/a = 2$, 4 and 8 cases.

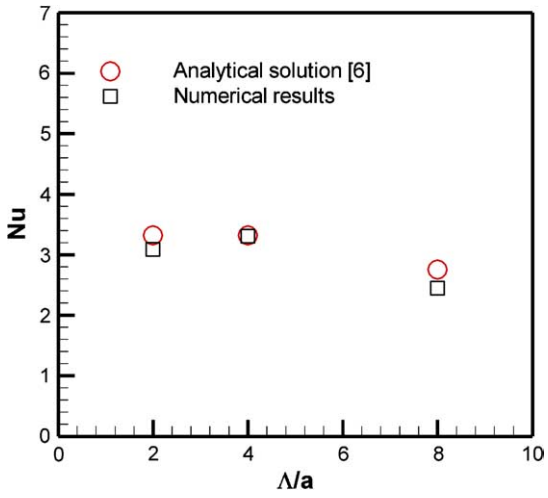

Fig. 5. The comparisons of Nusselt number at fully developed condition by numerical prediction and analytical solution for $\Lambda/a = 2$, 4 and 8 cases.

4.2. Distributions of entropy generation for baseline cases with $\Lambda/a = 4$

For understanding the development of entropy generation in the duct, the contours of entropy generation, S'''_{gen}, on cross-sectional planes at $z/a = 2$, 4, 6 and 8 for $\Lambda/a = 4$ case with $q'' = 320$ W/m^2, $Re = 172$; $q'' = 320$ W/m^2, $Re = 860$; and $q'' = 640$ W/m^2, $Re = 860$ are shown in Fig. 6(a)–(c), respectively. It can be found the principal distribution shows similar patterns in all cases, and the most serious entropy generation concentrates in the sharp corner where the upper and lower waved walls joint together. Near the central core of the duct, the entropy generation has relatively small magnitude. These results come from that the velocity gradient as well as the temperature gradient is serious near the sharp corner, but gentle near the central core. Although the magnitudes of entropy generation increases or decreases in different regions as the flow develops, the changes of the entropy generation from upstream to downstream are not significant. Nonetheless, the core region with smaller entropy generation is found to gradually shrink inwardly as the flows develop toward downstream. The effects of Re on entropy generation can be investigated from the comparison of Fig. 6(a) and (b), from which the entropy generation in the sharp corner is found to increase with Re, whereas the entropy in the central core decreases. The results are due to the opposite influences of the increase of Re on entropy generation from frictional irreversibility and heat transfer irreversibility. As described in Eq. (9), entropy can be generated from the

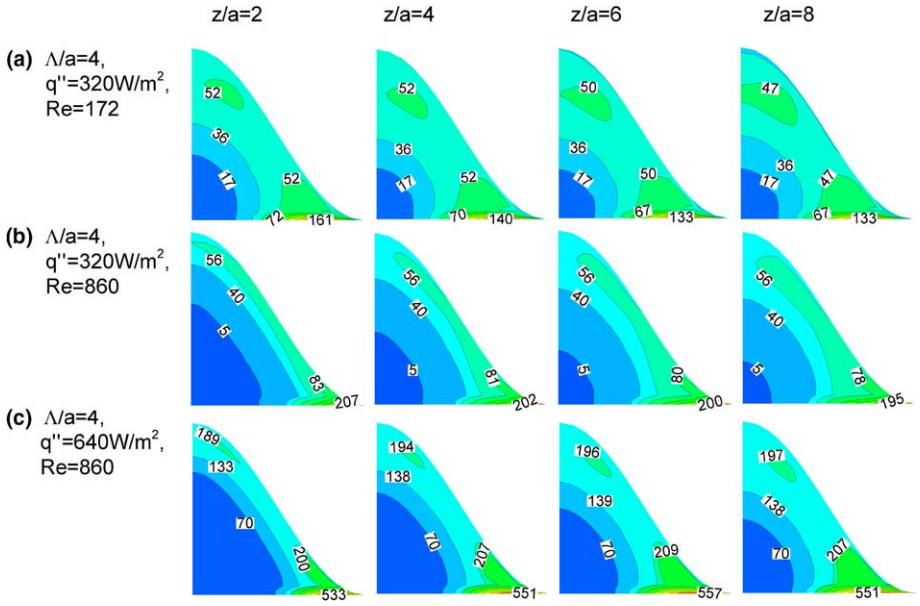

Fig. 6. The contours of entropy generation, S'''_{gen}, on cross-sectional planes at $z/a = 2$, 4, 6 and 8 for $\Lambda/a = 4$ case: (a) $q'' = 320$ W/m^2, $Re = 172$; (b) $q'' = 320$ W/m^2, $Re = 860$; (c) $q'' = 640$ W/m^2, $Re = 860$.

irreversibility of fluid friction and the heat transfer. When Re increases, both of the fluid friction and heat transfer coefficient will increase. The increase of fluid friction results the increase of entropy generation, S'''_P, whereas the increase of heat transfer coefficient makes the temperature distribution become smoother, and thus reduces the entropy generation, S'''_T. The competition of S'''_P and S'''_T in the flow fields determines the final changes of the resultant entropy generation, S'''_{gen}. The influences of heat flux on entropy generation can be detected from the comparison of Fig. 6(b) and (c). Clearly, the increase of heat flux is found to cause the increase of entropy generation in whole flow fields, which is attributed to the more serious irreversibility due to the larger heat transfer.

4.3. Effects of Re and q'' on S^*_P and S^*_T for $\Lambda/a = 4$ case

In the following, the non-dimensional entropy generation rate, S^*_P, S^*_T and S^*_{gen}, in whole chevron channel are defined by

$$S^*_P = \frac{\int_V S'''_P \mathrm{d}V}{\dot{Q}/T_0}, \quad \text{and} \quad S^*_T = \frac{\int_V S'''_T \mathrm{d}V}{\dot{Q}/T_0} \quad S^*_{\text{gen}} = \frac{\int_V S'''_{\text{gen}} \mathrm{d}V}{\dot{Q}/T_0}$$

where V is the total volume of the computational domain. For evaluating the entropy generation in whole flow fields, the total entropy generation in the channel, S^*_{gen}, will be analyzed. However, for clear understanding of the influences of Re on the resultant entropy generation, the entropy generated from heat transfer (S^*_T) and fluid friction (S^*_P) will be analyzed separately first. Fig. 7 shows the relationship between the entropy generation and Re for $\Lambda/a = 4$ case. When Re increases, it can be found from the figure, S^*_P increases and S^*_T decreases in all heat flux cases. The increase of S^*_P with the increase of Re is attributed to the frictional irreversibility will become more serious as Re becomes larger, whereas S^*_T is reduced in larger Re cases since the heat transfer coefficient will be enhanced by the larger Re and the temperature gradient in the flow field will accordingly become more gentle. Because of the incompressible assumption, the velocity fields will remain the same and independent on the heat flux. Therefore, S'''_P, which is mainly related with the velocity gradient, will not be significantly affected by heat flux. However, due to the normalization of $\dot{Q}/T_0$ and temperature term appears in the dominator of S'''_P, S^*_P is induced to become larger in the smaller q'' cases, no matter the magnitudes of Re. In addition, the more serious heat transfer irreversibility caused by the larger q'' results the larger S^*_T for all Re cases. Fig. 7 also points out the competition between the magnitudes of S^*_P and S^*_T is dependent on Re and q''. For $q'' = 160$ and 320 w/m^2 cases, S^*_P and S^*_T curves intersect each other at $Re = 832$ and 1456, respectively. For the cases with Re less than the intersectional Re, S^*_T is larger than S^*_P, and vice verse when Re exceeds the intersectional Re. Comparing the two heat flux cases, the Re region where S^*_T is larger than S^*_P, becomes wider as q'' increases. For the case with

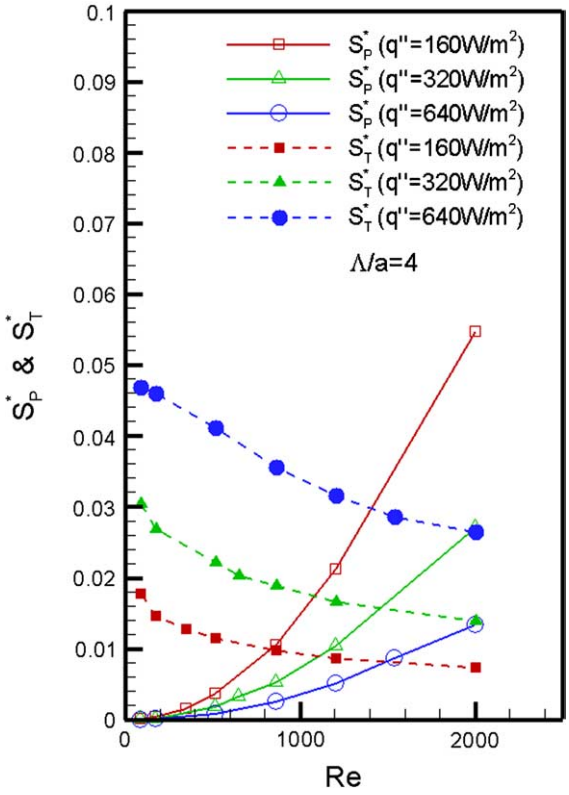

Fig. 7. The effects of Re on the entropy generation generated from heat transfer (S^*_T) and fluid friction (S^*_P) for $\Lambda/a = 4$ case.

$q'' = 640$ w/m^2, S^*_T becomes larger thanS^*_P in all Re cases calculated in the current study. These results clearly reveal that S^*_P is the dominant source of the entropy generation in flow fields for cases with high Re and small q'', while the dominant source is S^*_T for cases with low Re and large q''. Such results provide worthy information to catch the impression about the major source that the entropy generation comes from.

4.4. Effects of Re on S^*_{gen} and optimal Re analysis for $\Lambda/a = 4$ case

Fig. 8 shows the relationship between S^*_{gen} and Re for $\Lambda/a = 4$ cases with different q''. The figure indicates clearly S^*_{gen} is not monotonically related with q'' or Re. For smaller Re cases ($Re < 1069$), S^*_{gen} is larger in the larger q'' cases since S^*_T is the dominant term and it increases with q''. For larger Re cases ($Re > 1895$), S^*_{gen} becomes larger in smaller q'' cases, which is resulted from S^*_P is the dominant term and it is larger in the smaller q'' cases. Since neither S^*_P nor S^*_T is the dominant term for the medium Re ($1069 < Re < 1895$) case, the relationship between S^*_{gen} and q'' becomes not monotonic. Nonetheless, there exists optimal Re with the minimal S^*_{gen} for every q'' case obviously, and the optimal Re is found to increase with q''. Fig. 9 shows the optimal Re for different q'' cases. The optimal Re for $q'' = 160$, 320 and 640 w/m^2 cases are 350, 660 and 1204, respectively.

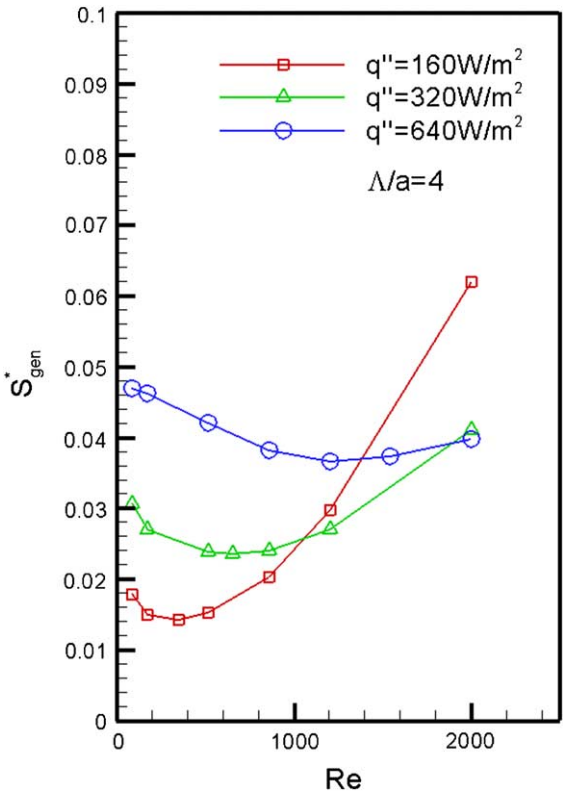

Fig. 8. The relationship between entropy generation, S^*_{gen}, and Re for $\Lambda/a = 4$ cases with different q''.

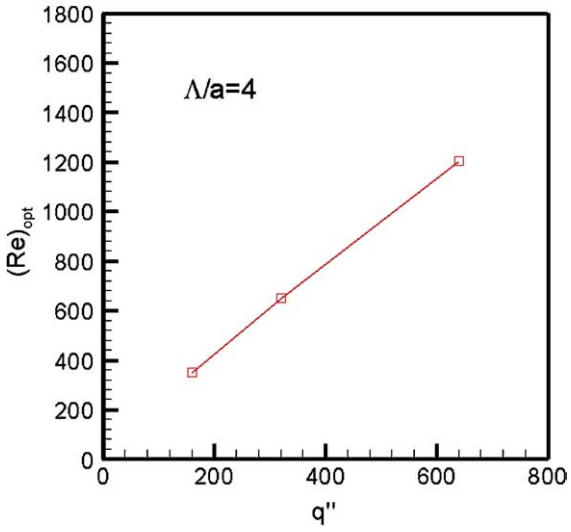

Fig. 9. The optimal Re for $\Lambda/a = 4$ cases with different q'' cases.

4.5. Effects of aspect ratio

Fig. 10(a) and (b) show the contours of volumetric entropy generation, S'''_{gen}, on cross-sectional planes at $z/a =$ 2, 4, 6 and 8 for cases of $q'' = 320$ W/m^2, $Re = 860$ with $\Lambda/a = 2$, and 8, respectively. Through the comparison from Fig. 10(a), (b) and Fig. 6(b), the effects of aspect ratio on the entropy generation can be detected. For all aspect ratio cases, the most serious entropy generation concentrates near the sharp corner, and the maximum S'''_{gen} occurs in $\Lambda/a = 4$ case, whereas the minimum occurs in $\Lambda/a = 2$ case. For every aspect ratio case, the central core of the duct remains as the region with smaller entropy generation, and the core region tends to gradually shrink inwardly as the flow develops toward downstream.

Fig. 11(a)–(c) show the influences of Reynolds number on S^*_P and S^*_T for different aspect ratio cases with $q'' = 160$, 320 and 640 W/m^2, respectively. For all Re cases with different q'', S^*_P is found to be minimal in $\Lambda/a = 2$ case, whereas S^*_T is minimal in $\Lambda/a = 4$. In general, the trend that the entropy generation in the case with high Re and small q'' is dominated by S^*_P; whereas S^*_T is the dominant source of entropy generation in cases with low Re and large q'' cases, remains the same for all aspect ratio cases. Fig. 12(a)–(c) show the relationship between S^*_{gen} and Re for different Λ/a cases with $q'' = 160$, 320 and 640 W/m^2, respectively. A clear trend can be found for all Λ/a cases through the comparison between the figures that the largest S^*_{gen} appears in the higher Re side for $q'' = 160$ W/m^2 case, whereas the largest S^*_{gen} location gradually transfers toward the lower Re side as q'' increases to 320 and 640 W/m^2.

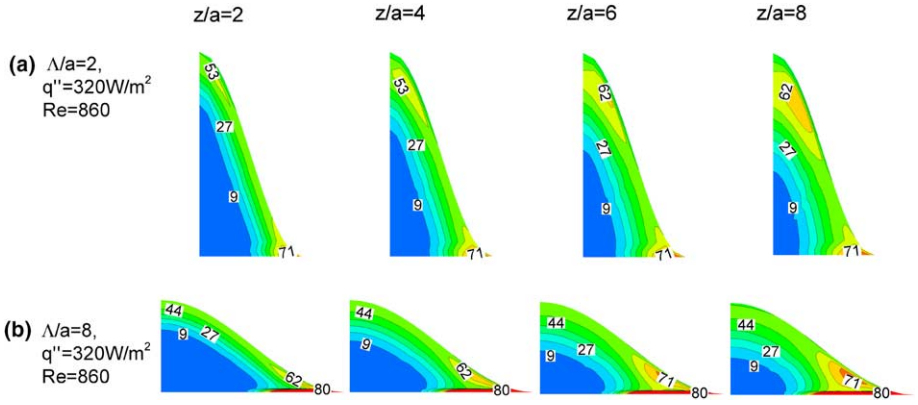

Fig. 10. The contours of volumetric entropy generation, S'''_{gen}, on cross-sectional planes at $z/a = 2$, 4, 6 and 8 for cases of $q'' = 320$ W/m^2, $Re = 172$ with (a) $\Lambda/a = 2$; and (b) $\Lambda/a = 8$.

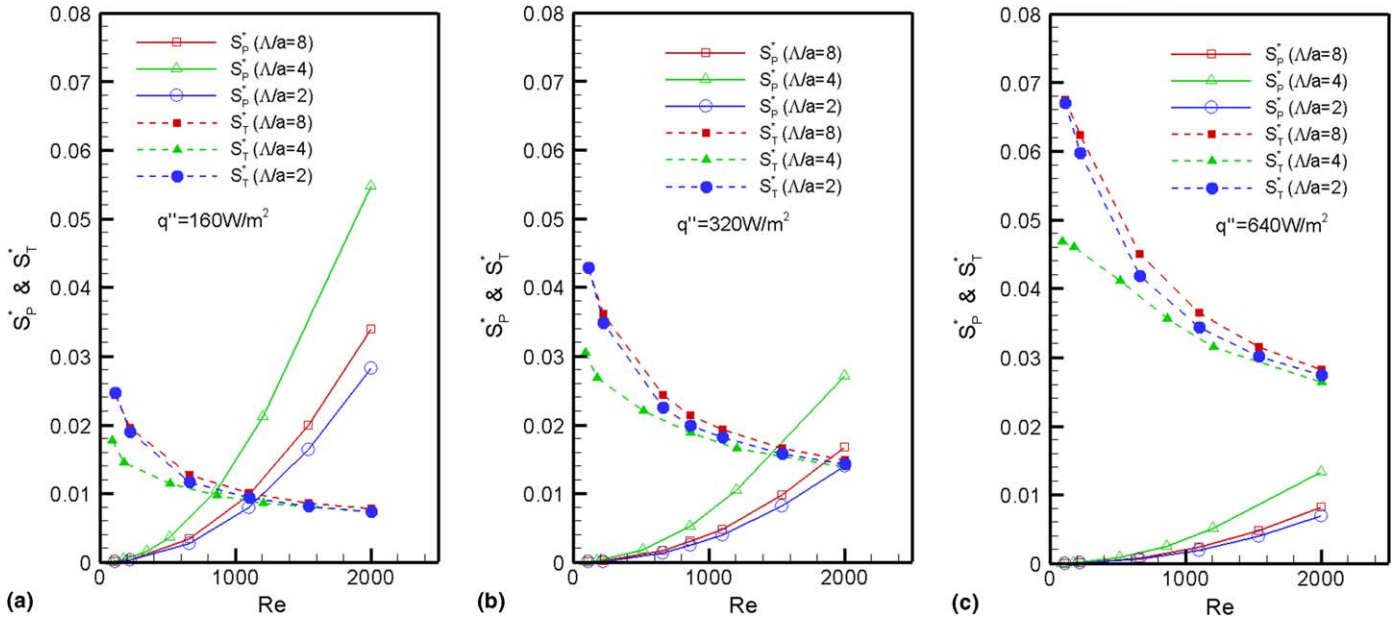

Fig. 11. The effects of Reynolds number on S_P^* and S_T^* for different aspect ratio cases: (a) $q'' = 160$ W/m^2; (b) $q'' = 320$ W/m^2; and (c) $q'' = 640$ W/m^2.

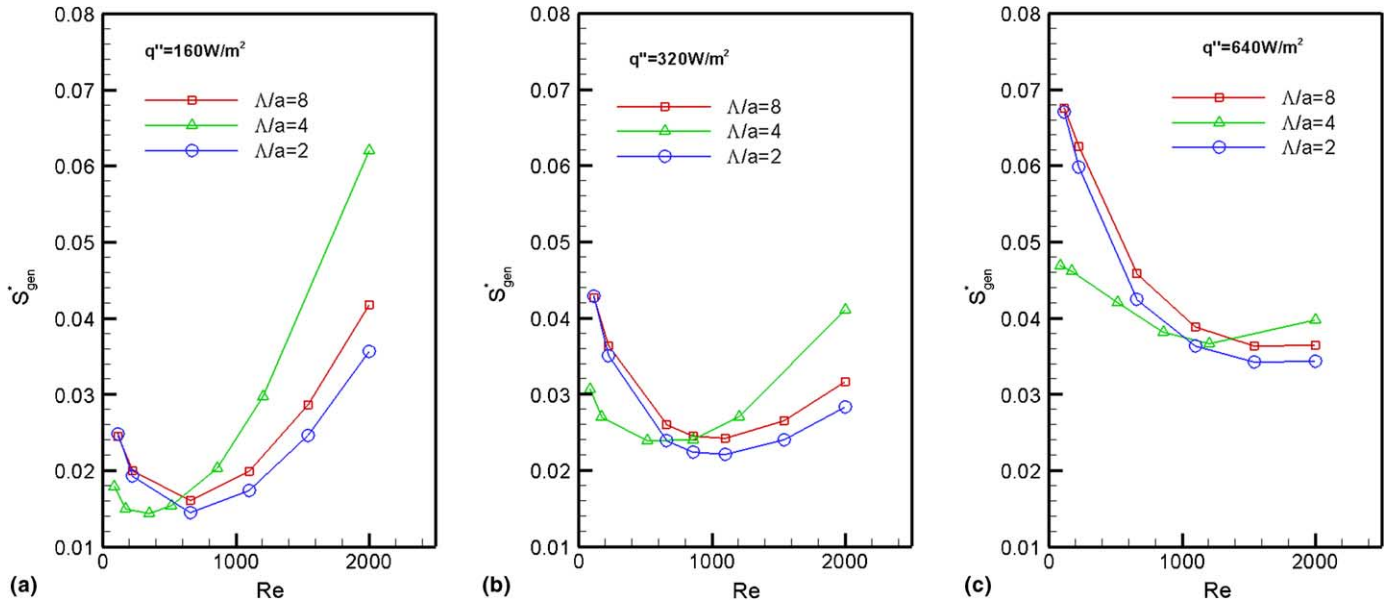

Fig. 12. The relationship between entropy generation, S_{gen}''', and Re for different Λ/a cases: (a) $q'' = 160$ W/m^2; (b) $q'' = 320$ W/m^2; and (c) $q'' = 640$ W/m^2.

Such developments reveal the fact that S_P^* is the major source of S_{gen}^* for smaller q'' case, so that the greatest S_{gen}^* will appear in the higher Re side since the higher Re will cause more serious frictional irreversibility and the resultant S_P^*. For larger q'' case, the dominant entropy generation becomes S_T^*, which results the largest S_{gen}^* transfers toward the low Re region since the low heat transfer coefficient in low Re cases will induce serious temperature gradient and the corresponding entropy generation, S_T^*. In addition, Fig. 12(a)–(c) also point out the important influence of Λ/a on S_{gen}^*, from which the optimal aspect ratio, $(\Lambda/a)_{\text{opt}}$, with which the minimal induced S_{gen}^* can be obtained, is found to be dependent on Re and q''. In $q'' = 160$ W/m^2 case, $(\Lambda/a)_{\text{opt}} = 2$ when $Re > 540$; $(\Lambda/a)_{\text{opt}} = 4$ when $Re < 540$. Similar situations can be found in $q'' = 320$ and 640 W/m^2 cases. In $q'' = 320$ W/m^2 case, $(\Lambda/a)_{\text{opt}} = 2$ when $Re > 662$; $(\Lambda/a)_{\text{opt}} = 4$ when $Re < 662$. In $q'' = 640$ W/m^2 case, $(\Lambda/a)_{\text{opt}} = 2$ when $Re > 1008$; $(\Lambda/a)_{\text{opt}} = 4$ when $Re < 1008$. One thing worthy of special caution from the observation of Fig. 12(a)–(c) is there exists an optimal Re for every Λ/a case to induce the minimal S_{gen}^*. Fig. 13 shows the relationship between optimal Re and Λ/a for cases with different q'', from which the optimal Re is found to increase as q'' increases. These results

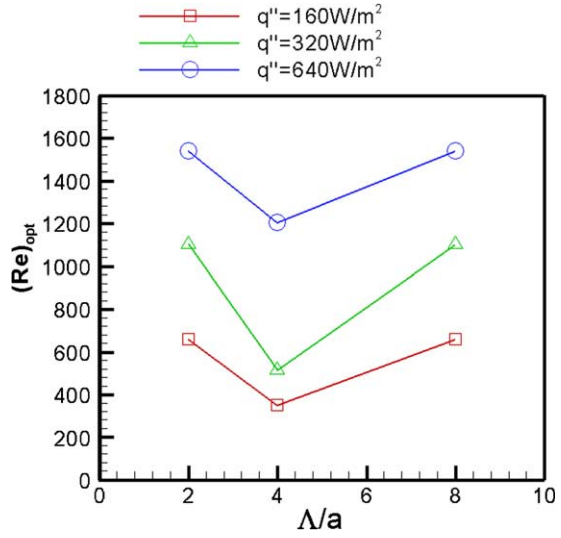

Fig. 13. The relationship between optimal Re and Λ/a for cases with different q''.

provide important information for the heat exchanger design since the optimal Re and optimal aspect ratio are suggested to be used according to the practical design conditions so that the thermal system could have the least irreversibility and the best exergy utilization.

5. Conclusions

The entropy generation in a double-sine duct with various Re and q'' is investigated by numerical methods. The effect of aspect ratio is also included in current studies. The results show that S_P^* will become more dominated in cases with larger Re and smaller q'', while S_T^* will become more dominated in cases with smaller Re and larger q''. For the cases if S_P^* is dominant, S_{gen}^* is larger in smaller q'' cases; meanwhile, for the cases if S_T^* is dominant, S_{gen}^* is larger in larger q'' cases. For all Re cases with different q'', there is no monotonic relationship between Λ/a and S_P^* or S_T^*. S_P^* is found to be minimal in $\Lambda/a = 2$ case, whereas S_T^* is minimal in $\Lambda/a = 4$ case. The optimal aspect ratio, $(\Lambda/a)_{\text{opt}}$, with which the minimal induced S_{gen}^* can be obtained, is dependent on Re and q''. In $q'' = 160\ \text{W/m}^2$ case, $(\Lambda/a)_{\text{opt}} = 2$ when $Re > 540$; $(\Lambda/a)_{\text{opt}} = 4$ when $Re < 540$. In $q'' = 320\ \text{W/m}^2$ case, $(\Lambda/a)_{\text{opt}} = 2$ when $Re > 662$; $(\Lambda/a)_{\text{opt}} = 4$ when $Re < 662$. In $q'' = 640\ \text{W/m}^2$ case, $(\Lambda/a)_{\text{opt}} = 2$ when $Re > 1008$; $(\Lambda/a)_{\text{opt}} = 4$ when $Re < 1008$. There exists an optimal Re for every case with specific Λ/a and q'' case to induce the minimal S_{gen}^*, and the optimal Re is found to increase as q'' increases. These results provide important information for the heat exchanger design since the thermal system could have the least irreversibility and best exergy utilization if the optimal Re and optimal aspect ratio can be used according to the practical design conditions.

References

[1] R.K. Shah, W.W. Focke, Plate heat exchangers and their design theory, in: R.K. Shah, E.C. Subbarao, R.A. Mashelkar (Eds.), Heat Transfer Equipment Design, Hemisphere Publishing Co., Washington, DC, 1988, pp. 227–254.
[2] W.W. Focke, J. Zachariades, I. Olivier, The effect of the corrugation inclination angle on the thermohydraulic performance of plate heat exchangers, Int. J. Heat Mass Transfer 28 (8) (1985) 1469–1479.
[3] R.L. Heavner, H. Kumar, A.S. Wannizrachi, Performance of an industrial plate heat exchanger: effect of chevron angle, AICHE Symp. Ser. 89 (295) (1993) 65–70.
[4] H. Martin, A theoretical approach to predict the performance of chevron-type plate heat exchangers, Chem. Eng. Process. 35 (1996) 301–310.
[5] J. Ding, H. Manglik, Analytical solutions for laminar fully developed flows in double-sine shaped ducts, Heat Mass Transfer 31 (1996) 267–277.
[6] R.M. Manglik, J. Ding, Laminar flow heat transfer to viscous power-law fluids in double-sine ducts, Int. J. Mass Heat Transfer 40 (6) (1997) 1379–1390.
[7] L. Fisher, H. Martin, Friction factors for fully developed laminar flow in ducts confined by corrugated parallel walls, Int. J. Heat Mass transfer 40 (3) (1997) 635–639.
[8] J.Y. Jang, C.N. Lin, A numerical analysis of three-dimensional heat transfer and fluid flow in chevron plate channels, ASHPAE Trans.: Symposia, MN-00-14-2, pp. 856–863.
[9] A. Bejan, Entropy Generation Minimization, CRC Press, Boca Raton, FL, 1996.
[10] A. Bejan, Entropy Generation Through Heat and Fluid Flow, Wiley, New York, 1982.
[11] P.K. Nag, K. Naresh, Second law optimization of convection heat transfer through a duct with constant heat flux, Int. J. Energy Res. 13 (1989) 537–543.
[12] A.Z. Sahin, Irreversibilities in various duct geometries with constant wall heat flux and laminar flow, Energy 23 (6) (1998) 465–473.
[13] A.Z. Sahin, Thermodynamics of laminar viscous flow through a duct subjected to constant heat flux, Energy 21 (12) (1996) 1179–1187.
[14] S.Z. Shuja, Optimal fin geometry based on exergoeconomic analysis for a pin-fin array with application to electronics cooling, Exergy 2 (2002) 248–258.
[15] T.H. Ko, K. Ting, Entropy generation and thermodynamic optimization of fully developed laminar convection in a helical coil, Int. Commun. Heat Mass Transfer 32 (2005) 214–223.
[16] T.H. Ko, K. Ting, Optimal Reynolds number for the fully developed laminar forced convection in a helical coiled tube, Energy: The Int. J., accepted for publication.
[17] T.H. Ko, Numerical investigation of laminar forced convection and entropy generation in a helical coil with constant wall heat flux, Numer. Heat Transfer, Part A, accepted for publication.
[18] B.E. Launder, D.B. Spalding, The numerical computation of turbulent flows, Comput. Methods Appl. Mech. Eng. 3 (1974) 269–289.
[19] S.V. Partankar, Numerical Heat Transfer and Fluid Flow, Hemisphere, Washington, DC, 1980.